

NUMERICAL INVESTIGATIONS OF THE NATURE OF THE FIRST BIFURCATION FOR THE FLOW IN AN ANNULAR ROTOR/STATOR CAVITY

EWA TULISZKA-SZNITKO
ARTUR ZIELIŃSKI

*Institute of Thermal Engineering, Technical University of Poznań
e-mail: sznitko@sol.put.poznan.pl*

Direct numerical simulation is performed to study a transitional flow in an annular rotating cavity of different aspect ratios $L = 4.0, 5.0$ and different curvature parameters $R_m = (R_1 + R_0)/(R_1 - R_0) = 1.5 - 6.0$. This paper reports on the influence of the curvature parameter R_m and end-wall boundary layers on the nature of the first bifurcation to unsteadiness and on instability structures in the rotor and stator boundary layers. For all considered end-wall boundary conditions, we have observed clearly supercritical transition to unsteadiness for larger R_m and direct transition from a steady flow to chaotic one for small R_m . A spectral collocation method based on the Chebyshev polynomial is used for solving the incompressible Navier-Stokes equations. The time scheme is semi-implicit and second-order accurate; it corresponds to a combination of the second-order backward differentiation formula for the viscous diffusion terms and the Adams-Bashforth scheme for the non-linear terms. The method uses a projection scheme to maintain the incompressibility constraint.

Key words: rotating cavity, direct method, laminar-turbulent transition

1. Introduction

Flow in a rotating cavity is very important from both theoretical and practical points of view. Typical industrial configurations are cavities between compressors and turbine disks. From the theoretical point of view, it is also important to understand the sequence of consecutive bifurcations through which the initially steady flow undergoes transition to turbulence as the Reynolds number increases. Numerous works have been recently devoted to the

investigation of instabilities associated with flow in a single rotating disk (Kobayashi *et al.*, 1980; Lingwood 1995, 1996, 1997) and to flow between different rotating disks (Daube *et al.*, 2001; Itoh, 1991; Tuluszka-Sznitko and Soong, 2000; Tuluszka-Sznitko *et al.* 2002; Serre *et al.*, 2001, 2004; Serre and Pulicani, 2001; Cousin-Rittemard, 1996; Cousin-Rittemard *et al.*, 1998). In the case of rotor/stator flows, at high rotational rates, the flow consists of two boundary layers (on the rotating and stationary disk) separated by an inviscid rotating core. The transition process in both boundary layers is related to type I and type II generic linear instabilities. Type I instability is due to the presence of an inflection point in the boundary layer velocity profile. The mechanism for type II instability is related to combined effects of Coriolis and viscous forces. Fallor (1963), Caldwell and Van Atta (1970) investigated experimentally type I and type II instabilities in the Ekman flow and found reasonably good agreement with the linear stability theory. Savas (1987) studied experimentally unsteady uniformly rotating flow over a stationary disk and found both rings and spiral structures recognised as type II and type I instability, respectively. In the rotor/stator cavity flow and in flows around a single rotating disk, experimental results exhibit similar instability structures. However, the confinement of the geometry (rotor/stator geometry) has effect on the critical Reynolds number. Large influence of the end-wall boundary conditions also has been reported. The influence of the attachment of the end-wall to the rotor or to the stator has been investigated by many authors, Adams and Szeri (1982), Dijkstra and Heijst (1983), Cousin-Rittemard (1996), Cousin-Rittemard *et al.* (1998), Oliveira *et al.* (1991).

In the present paper, we focused attention on the first bifurcation of the flow in an annular rotor/stator cavity. Calculations are performed using highly precise spectral collocation method based on the Chebyshev polynomials. The study of the first stage of transition to turbulence using DNS is vital because this method allows for an accurate description of the instability mechanisms which are known to play an important role in the breakdown process to turbulence. The nature of the first bifurcation of the flow in a cylindrical cavity of the aspect ratio $L = 5$ and $R_m = 1$ was investigated in detail in the paper by Serre *et al.* (2004). These 3D calculations showed, for the first time, that the transition to unsteadiness for a high aspect ratio ($L = 5$) in the cylindrical cavity is supercritical. Daube *et al.* (2001) performed 2D calculations to investigate nature of first bifurcations in annular cavity of the aspect ratio $L = 5$ and different curvature $R_m = 1.5 - 99.0$. He found that for larger R_m , the transition is supercritical and for small $R_m \approx 1.5$ is subcritical. In the present paper, we performed calculations for $L = 5$ and 4, for different R_m and for different end-wall boundary conditions to analyse the influence of end-

wall conditions on the nature of first bifurcations and instability structures. We restricted ourselves to a 2D flow to compare results obtained for linear end-wall profiles to those obtained by Daube *et al.* (2001).

In the following Sections 2, 3 and 4, we formulated the problem and briefly described the numerical method. The results are presented in Section 5, and concluding remarks are given in Section 6.

2. Geometrical model

The geometrical model is a rotor-stator annular cavity characterized by the aspect ratio $L = (R_1 - R_0)/2h$ and the curvature parameter $R_m = (R_1 + R_0)/(R_1 - R_0)$. The disks are bounded by cylinders of height $2h$, which can be stationary or rotating (Fig. 1).

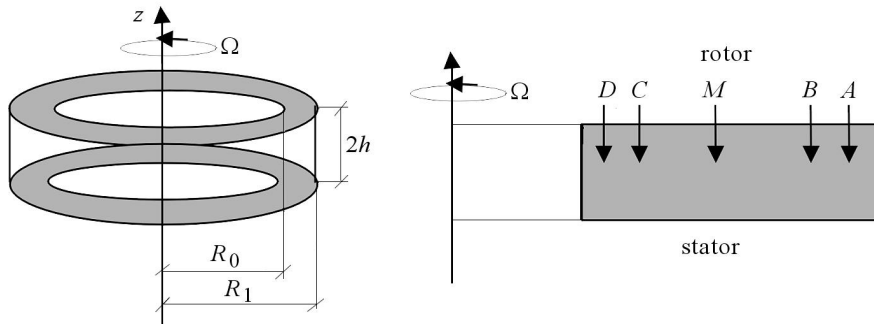


Fig. 1. (a) A scheme of the annular rotating cavity, (b) location of monitoring points in the radial direction

The rotor rotates with uniform angular velocity $\Omega = \Omega e_z$, where e_z denotes the unit vector. The origin of the z -axis is located at the mid-height between the disks. The governing parameters are:

- the Reynolds number based on the external radius of the disks is $\text{Re}_R = R_1^2 \Omega / \hat{\nu}$
- the Reynolds number based on the height of the cylinder is $\text{Re}_h = (2h)^2 \Omega / \hat{\nu}$
- the local Reynolds number based on the viscous scale $\delta = \sqrt{\hat{\nu} / \Omega}$ is:

$$\text{Re}_\delta = \frac{\delta r^* \Omega}{\hat{\nu}} = \sqrt{\frac{r^{*2} \Omega}{\hat{\nu}}}$$

where $\hat{\nu}$ is kinematic viscosity.

The asterisk denotes a dimensional value. The Reynolds number $\text{Re}_R = R_1^2 \Omega / \widehat{\nu}$ is the squared upper bound of the local Reynolds number $\text{Re}_\delta = \sqrt{r^{*2} \Omega / \widehat{\nu}}$. The local Reynolds number is used to discuss instability thresholds and characteristic parameters of instability waves.

3. Mathematical model

The governing equations are 2D Navier-Stokes equations written in velocity-pressure formulation together with the continuity equation. The equations are written in the cylindrical polar coordinate system (r, φ, z) , with respect to the stationary frame of reference

$$\begin{aligned} \frac{1}{L} \frac{\partial u}{\partial r} + \frac{u}{L(R_m + r)} + \frac{\partial w}{\partial z} &= 0 \\ \frac{\partial u}{\partial t} + L(R_m + 1)Au &= -(R_m + 1) \frac{\partial P}{\partial r} + \frac{L^2(R_m + 1)^2}{\text{Re}_R} \left[\Delta u - \frac{u}{L^2(R_m + r)^2} \right] \\ \frac{\partial v}{\partial t} + L(R_m + 1)Av &= \frac{L^2(R_m + 1)^2}{\text{Re}_R} \left[\Delta v - \frac{v}{L^2(R_m + r)^2} \right] \\ \frac{\partial w}{\partial t} + L(R_m + 1)Aw &= -L(R_m + 1) \frac{\partial P}{\partial z} + \frac{L^2(R_m + 1)^2}{\text{Re}_R} \Delta w \end{aligned} \quad (3.1)$$

where

$$\begin{aligned} Au &= \frac{1}{L} u \frac{\partial u}{\partial r} + w \frac{\partial u}{\partial z} - \frac{v^2}{L(R_m + r)} \\ Av &= \frac{1}{L} u \frac{\partial v}{\partial r} + w \frac{\partial v}{\partial z} - \frac{uv}{L(R_m + r)} \\ Aw &= \frac{1}{L} u \frac{\partial w}{\partial r} + w \frac{\partial w}{\partial z} \end{aligned} \quad (3.2)$$

The cylindrical Laplacian operator for a two-dimensional flow is defined in the following way

$$\Delta = \frac{1}{L^2} \frac{\partial^2}{\partial r^2} + \frac{1}{L^2(R_m + r)} \frac{\partial}{\partial r} + \frac{\partial^2}{\partial z^2} \quad (3.3)$$

where t is time, (u, v, w) are velocity \mathbf{V} components in the r , φ and z directions, respectively, P is pressure. The scales for dimensionless variables of

time and velocity are Ω^{-1} and ΩR_1 , respectively. The dimensionless axial co-ordinate is $z = z^*/h$; $z \in [-1, 1]$. The radius co-ordinate is normalised to obtain the domain $[-1, 1]$ requested by the spectral method based on the Chebyshev polynomials: $r = [2r^* - (R_1 + R_0)] / (R_1 - R_0)$. The boundary conditions are as follows: no slip boundary conditions at any rigid wall $u = w = 0$. For the azimuthal velocity component, the boundary conditions are: $v = 0$ on the stator and $v = (R_m + r) / (R_m + 1)$ on the rotating disk. On the stationary end-walls, the azimuthal velocity equals zero $v = 0$. However, because of the singularity of the azimuthal velocity at the junction between the stationary end-walls and rotating disk, this boundary condition must be modified. The singularity expresses a physical situation, in which there is a thin gap between the edge of the rotating disk and the stationary end-walls. To eliminate this singularity, different azimuthal velocity profiles are used for $r = \pm 1$: the linear profile $v = (1 + z)(R_m + r) / [2(R_m + 1)]$ (Serre and Pulicani, 2001) and the exponential profile $v = [(R_m + r) / (R_m + 1)] \exp[(z - 1) / 0.006]$ (Serre *et al.*, 2004).

We proceed as follows: the rotation of the rotor is increased step by step with a small increment $\Delta \text{Re}_R = 2000$. The solution obtained for smaller Re_R is then used as the initial condition for computation with a higher Reynolds number. In the first iteration, as the initial condition we use a flow which corresponds to lack of motion in the meridional plane and to the linear azimuthal velocity profile: $u = 0$, $v = (1 + r)(z + 1) / 4$, $w = 0$. Computations start with a sufficiently low Reynolds number, e.g. $\text{Re}_R = R_1^2 \Omega / \hat{\nu} = 3000$ to obtain a steady flow. The steady flow solutions are expected when the convergence rate becomes smaller than 10^{-7}

$$\frac{1}{\Delta T} |\mathbf{V}^{n+1} - \mathbf{V}^n| \leq 10^{-7} \quad (3.4)$$

where ΔT is the time step.

4. Direct numerical simulation (DNS)

In this paper, we restrict ourselves to a 2D flow. A numerical solution is based on the spectral collocation method (Canuto *et al.*, 1988). The Gauss-Lobatto collocation points are used

$$\begin{aligned} r_i &= \cos \frac{i\pi}{N} & z_j &= \cos \frac{j\pi}{M} & i &= 0, 1, \dots, N \\ & & & & j &= 0, 1, \dots, M \\ & & & & (r_i, r_j) &\in [-1, 1] \times [-1, 1] \end{aligned} \quad (4.1)$$

where N and M are the number of collocation points in the radial and axial directions, respectively. The solution $\Psi = (u, w, v, P)$ of equations (3.1) is approximated by means of an expansion of the Chebyshev polynomials in the r and z directions (Serre *et al.*, 2001; Serre and Pulicani, 2001)

$$\Psi(r, z) = \sum_{n=0}^N \sum_{m=0}^M \Psi_{nm} T_n(r) T_m(z) \quad \text{for} \quad r, z \in [-1, 1] \quad (4.2)$$

The time scheme is semi-implicit and second-order accurate. It corresponds to a combination of the second-order backward differentiation formula for the viscous diffusion term and the Adams-Bashforth scheme for the non-linear terms. The method uses the projection scheme to maintain the incompressibility constraint. Details are described in Serre *et al.* (2001), Serre and Pulicani (2001).

4.1. Predictor

The first task is to find the pressure distribution. The pressure predictor P^p is computed from the pressure elliptic equation derived from continuity equation (3.1)₁ and Navier-Stokes equations (3.1)₂ - (3.1)₄

$$\Delta P^p = -\text{Div } N(\mathbf{V}) \quad (4.3)$$

where $N(\mathbf{V})$ denotes the non-linear terms of Navier-Stokes equations

$$N(\mathbf{V}) = [(N(\mathbf{V}))_r, (N(\mathbf{V}))_\varphi, (N(\mathbf{V}))_z]^\top$$

For the numerical purpose and 2D flow, we write this equation in the following way

$$\begin{aligned} & \frac{1}{L^2} \frac{\partial^2 P^p}{\partial r^2} + \frac{1}{L^2(R_m + r)} \frac{\partial P^p}{\partial r} + \frac{\partial^2 P^p}{\partial z^2} = \\ & = -2 \left(\frac{1}{L} \frac{\partial}{\partial r} A u^n + \frac{1}{L} \frac{1}{R_m + r} A u^n + \frac{\partial}{\partial z} A w^n \right) + \\ & + \left(\frac{1}{L} \frac{\partial}{\partial r} A u^{n-1} + \frac{1}{L} \frac{1}{R_m + r} A u^{n-1} + \frac{\partial}{\partial z} A w^{n-1} \right) \end{aligned} \quad (4.4)$$

where n , and $n - 1$ denote values obtained from the two previous consecutive iterations. Equation (4.4) is solved with the following boundary conditions

$$\begin{aligned} \frac{\partial P^p}{\partial r} &= -L(2Au^n - Au^{n-1}) + \frac{L^2(R_m + 1)}{\text{Re}_R} \cdot \\ &\cdot \left[2 \left(\Delta u^n - \frac{u^n}{L^2(R_m + r)^2} \right) - \left(\Delta u^{n-1} - \frac{u^{n-1}}{L^2(R_m + r)^2} \right) \right] \end{aligned} \quad (4.5)$$

$$\frac{\partial P^p}{\partial z} = -(2Aw^n - Aw^{n-1}) + \frac{L(R_m + 1)}{\text{Re}_R} (2\Delta w^n - \Delta w^{n-1})$$

The velocity predictor is calculated from the following equations

$$\begin{aligned} \Delta u^p - u^p \frac{1}{L^2(R_m + r)^2} - \frac{\text{Re}_R}{L^2(R_m + 1)^2} \frac{3}{2} \frac{u^p}{\Delta t} &= \frac{\text{Re}_R}{L^2(R_m + 1)^2} \cdot \\ &\cdot \left[\frac{-4u^n + u^{n-1}}{2\Delta t} + L(R_m + 1)(2Au^n - Au^{n-1}) + (R_m + 1) \frac{\partial P^p}{\partial r} \right] \\ \Delta v^p - v^p \frac{1}{L^2(R_m + r)^2} - \frac{\text{Re}_R}{L^2(R_m + 1)^2} \frac{3}{2} \frac{v^p}{\Delta t} &= \\ &= \frac{\text{Re}_R}{L^2(R_m + 1)^2} \left[\frac{-4v^n + v^{n-1}}{2\Delta t} + L(R_m + 1)(2Av^n - Av^{n-1}) \right] \\ \Delta w^p - \frac{\text{Re}_R}{L^2(R_m + 1)^2} \frac{3}{2} \frac{w^p}{\Delta t} &= \frac{\text{Re}_R}{L^2(R_m + 1)^2} \cdot \\ &\cdot \left[\frac{-4w^n + w^{n-1}}{2\Delta t} + L(R_m + 1)(2Aw^n - Aw^{n-1}) + L(R_m + 1) \frac{\partial P^p}{\partial z} \right] \end{aligned} \quad (4.6)$$

The boundary conditions for the above equations are as follow

$$u^p = u^{n-1} \quad v^p = v^{n-1} \quad w^p = w^{n-1} \quad (4.7)$$

4.2. Corrector

Corrections of the pressure and velocity are calculated from the following equations

$$\begin{aligned} \frac{3}{2\Delta t} (u^{n+1} - u^p) &= -(R_m + 1) \left(\frac{\partial P^{n+1}}{\partial r} - \frac{\partial P^p}{\partial r} \right) \\ \frac{3}{2\Delta t} (v^{n+1} - v^p) &= 0 \\ \frac{3}{2\Delta t} (w^{n+1} - w^p) &= -(R_m + 1) L \left(\frac{\partial P^{n+1}}{\partial z} - \frac{\partial P^p}{\partial z} \right) \end{aligned} \quad (4.8)$$

and

$$\frac{1}{L} \frac{\partial u^{n+1}}{\partial r} + \frac{u^{n+1}}{L(R_m + r)} + \frac{\partial w^{n+1}}{\partial z} = 0 \quad (4.9)$$

The boundary conditions for equations (4.9) are

$$\mathbf{V}^{n+1} \cdot \mathbf{n} = \mathbf{V}^p \cdot \mathbf{n} \quad (4.10)$$

We calculate u^{n+1} , v^{n+1} , w^{n+1} , P^{n+1} by introducing a new value

$$\phi = \frac{2\Delta t}{3}(P^{n+1} - P^n) \quad (4.11)$$

to equations (4.8)-(4.9). Finally, we obtain

$$\begin{aligned} & \frac{1}{L^2} \frac{\partial^2 \phi}{\partial r^2} + \frac{1}{L^2(R_m + r)} \frac{\partial \phi}{\partial r} + \frac{\partial^2 \phi}{\partial z^2} = \\ & = \frac{1}{L(R_m + 1)} \left[\frac{1}{L} \frac{\partial u^p}{\partial r} + \frac{u^p}{L(R_m + r)} + \frac{\partial w^p}{\partial z} \right] \end{aligned} \quad (4.12)$$

The boundary condition for this equation is

$$\text{Grad } \phi \cdot \mathbf{n} = 0 \quad (4.13)$$

The corrected pressure and velocity are as follow

$$\begin{aligned} P^{n+1} &= P^p + \frac{3}{2\Delta t} \phi & u^{n+1} &= u^p - (R_m + 1) \frac{\partial \phi}{\partial r} \\ v^{n+1} &= v^p & w^{n+1} &= w^p - (R_m + 1)L \frac{\partial \phi}{\partial z} \end{aligned} \quad (4.14)$$

At every new time level $[(n+1)\Delta t]$, each flow variable $\Psi(u^p, v^p, w^p, P^p, \phi)$ is a solution to a 2D equation of the following form (Serre and Pulicani, 2001)

$$\frac{1}{L^2} \frac{\partial^2 \Psi}{\partial r^2} + \frac{1}{L^2(R_m + r)} \frac{\partial \Psi}{\partial r} + \frac{\partial^2 \Psi}{\partial z^2} - \lambda \Psi = S \quad (4.15)$$

where λ is a constant. The above equation is approximated by the spectral collocation method, and the right-hand side of equation (4.15) is evaluated by a standard spectral technique. Then, full diagonalization is used to solve (4.15) (Haldenwang *et al.*, 1984). For the annular cavity, the matrices of radial and axial operators are diagonalizable with real eigenvalues. Details of the technique can be found in Serre and Pulicani (2001) and Haldenwang *et al.* (1984).

5. Results

The main purpose of the paper is to investigate the influence of end-wall boundary conditions on the instability of flow and on the nature of the first bifurcation.

Numerical investigation has been performed for a rotating annular cavity with aspect ratios $L = 4$ and 5 , and with curvature parameters $R_m = 1.5 - 6$. Preliminary tests indicated that the spatial resolution (61×49) in (r, z) for the considered range of Reynolds numbers constitutes a good compromise between accuracy and computational cost. The incorporated time step Δt is assumed from $1 \cdot 10^{-3}$ to $5 \cdot 10^{-3}$. Velocity fluctuations are computed with respect to the average flow solution. The behaviour of dependent variables has been monitored at 15 points in five different positions in the radial direction $N(1/6, 1/3, 1/2, 2/3, 5/6)$ and in three positions in the axial direction $M(9/10, 1/2, 1/10)$, where N and M are numbers of collocation points in the radial and axial direction, respectively. The monitoring points in the radial direction are marked by letters A, B, M, C and D in Fig. 1.

The accuracy of the solution was assessed by considering different grids: (61×49) , (111×69) and (121×91) . We have found that solutions are almost identical with different meshes. To estimate precision of our results, we compared them to 2D structures obtained by Serre *et al.* (2001), Serre and Pulicani (2001) in his 3D computations ($L = 5$, $R_m = 4, 5$, $\text{Re}_R = 62500, 74250$) and to 2D results by Daube *et al.* (2001). We compared some characteristic features of 2D flow structures such as frequency, number of rolls across the radial extent of the cavity, radial wavelengths and we obtained very good agreement.

5.1. Basic state

At a small Reynolds number, for instance $\text{Re}_R = 3000$, the flow is steady and composed of two disjoint boundary layers (one on each disk) and of the central core flow. Bachelor showed that a rotating disk drives the fluid below the disk into uniform rigid rotation by means of the viscous effect. This uniformly rotating core gives then rise to shear layers. Exemplary profiles of three components of the velocity obtained at the monitoring point A, M and D are presented in Fig. 2a,b,c. We can see that the fluid is pumped radially outward along the rotating disk and radially inward along the stationary disk. Both boundary layers are separated by the core rotating with nearly steady rotation.

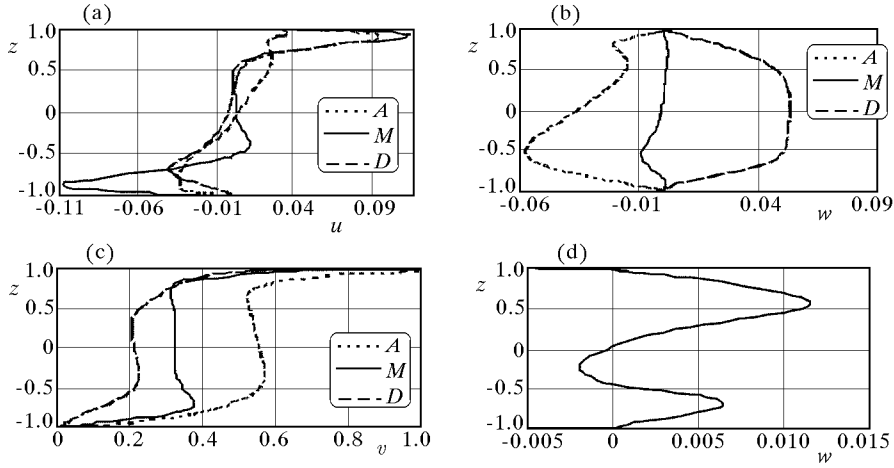


Fig. 2. Profiles of the radial u (a), axial w (b) and azimuthal v (c) velocity component obtained at the monitoring point A , M and D , $\text{Re}_R = 59000$, $L = 5$, $R_m = 4$, exponential end-wall azimuthal velocity profiles, the internal end-wall attached to the rotor and the outer end-wall attached to the stator, (d) azimuthal velocity profile obtained at the monitoring point D for $\text{Re}_R = 64000$, $L = 5$, $R_m = 4$, exponential end-wall azimuthal velocity profiles, both end-walls attached to the stator

5.2. Influence of end-wall conditions on instability structures in boundary layers ($L = 5$, $R_m = 4$)

In this section, we analyze the influence of the end-wall boundary conditions on the stability structures which appear in both rotating and stationary disk boundary layers.

As it was pointed out in Section 3, to eliminate singularity at the junctions between the stationary end-wall and rotating disk, the azimuthal velocity profile at the end-wall must be assumed. In our computations, we used two types of the end-wall profile:

- linear

$$v = (1 + z) \frac{R_m + r}{2(R_m + 1)} \quad \text{for } r = \pm 1 \quad (5.1)$$

- exponential:

– end-wall attached to the stator

$$v = \frac{R_m + r}{R_m + 1} \exp\left(\frac{z - 1}{0.006}\right) \quad \text{for } r = \pm 1 \quad (5.2)$$

– end-wall attached to the rotor

$$v = \frac{R_m + r}{R_m + 1} \left[1 - \exp\left(\frac{-z - 1}{0.006}\right) \right] \quad \text{for } r = \pm 1 \quad (5.3)$$

Figures 3a,b,c show, in the $(r^*/h, z)$ plane, instantaneous iso-lines of azimuthal velocity disturbances obtained for $\text{Re}_R = 60000$, $L = 5$, $R_m = 4$ and for the following end-wall boundary conditions:

- a) linear profiles for the shaft and shroud
- b) exponential profiles with both end-walls attached to the stator
- c) exponential profiles with the shaft attached to the rotor and with the shroud attached to the stator.

In Fig. 3a (case "a"; linear profiles for the shaft and shroud, $\text{Re}_R = 60000$) we observe 2 pairs of vortices in the boundary layer of the rotating disk propagate along the direction of the base flow (outward). In the boundary layer of the stationary disk we can see 5 pairs of counter-rotating vortices of the radial wave number $10 < \lambda_r^*/\delta < 29$, propagating inward with the phase speed $V_\phi^*/\Omega r^* \approx -0.1$. The radial wavelength of disturbances is defined as $\lambda_r^* = \Delta r^*/n_r$, where Δr is the radial length occupied by n_r rolls. Figure 3a shows that the disturbances in the boundary layer of the rotating disk are weaker than those in the stationary disk. The critical Reynolds number of the transition to unsteadiness equals $\text{Re}_R = 62500$.

In case "b" (both end-walls attached to the stator with exponential azimuthal end-wall profiles), we can see that only the boundary layer of the stationary disk is disturbed and that the stationary internal end-wall does not transport disturbances from the boundary layer of the stationary disk up to the rotating disk. As no disturbance can be transported between the layers from the stationary to rotating disk, the rotating disk remains stable and only very small oscillations can be observed.

Case "c" (the shaft attached to the rotor and the shroud attached to the stator with exponential azimuthal end-wall profiles) is the most unstable. In the boundary layer of the stationary disk we observe 6 pairs of vortices propagating inward. Then disturbances are transported up to the boundary layer of the rotating disk along the rotating end-wall. Figure 2b shows that the axial velocity component in the monitoring point D for case "a" is positive and is significantly different in character from the axial velocity profile in case "b" (Fig. 2d). Disturbed by vortices coming from the stator, the boundary layer of the rotating disk is unstable. In the boundary layer of the rotating disk we observe 2 pairs of strong counter-rotating vortices; amplitudes in the boundary

layers of the stationary and rotating disks are of the same order. Vortices in the rotating disk are propagated outward towards the outer stationary end-wall, which transports disturbances down to the stationary disk. The axial velocity component near the outer end-wall is negative (Fig. 2b). The critical Reynolds number of the first bifurcation equals 48750 and the angular frequency of disturbances in both boundary layers equals $\sigma = 2\pi/T \approx 4.2$ (where T is a time period taken from the instability characteristics).

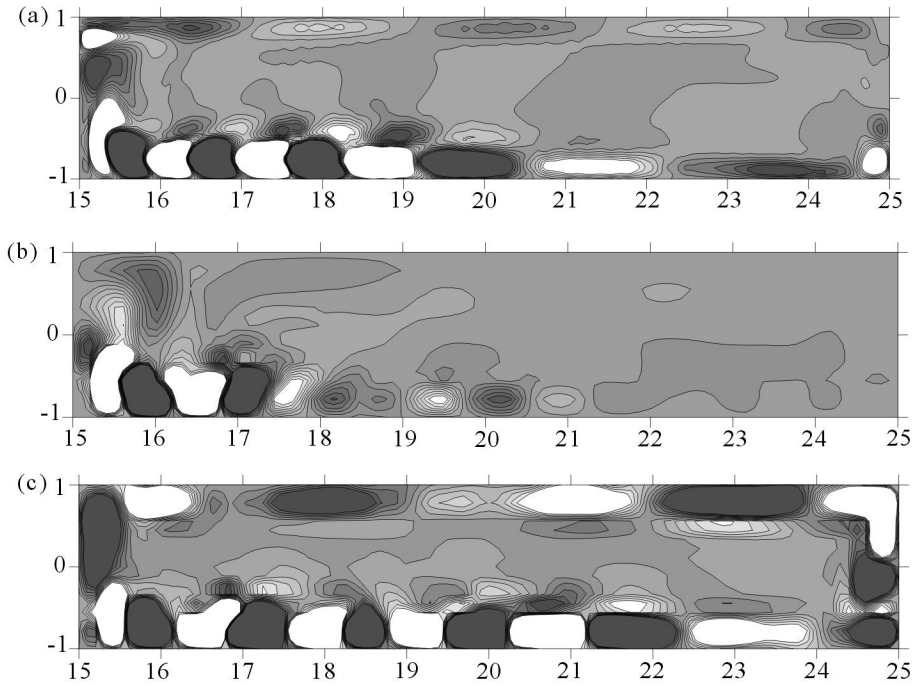


Fig. 3. Time dependent axisymmetric instability at $\text{Re}_R = 60000$, $L = 5$, $R_m = 4$. The iso-lines of disturbances of the azimuthal velocity component in the $(r^*/h, z)$ plane obtained for different end-wall boundary conditions. From the top to the bottom: (a) linear profiles for the shaft and shroud, (b) exponential profiles with both end-walls attached to the stator, (c) exponential profiles with the shaft attached to the rotor and with the shroud attached to the stator

5.3. Nature of the first bifurcation to unsteadiness

Stages of the transition to unsteadiness can be observed by analyzing the changes of dependent variables in terms of time obtained for consecutive Reynolds numbers. In the present paper, we analyze changes of the axial velocity component. Let us consider first the classical scenario of the transition. At

the beginning of the process, a change in rotation brings about a disturbance characterized by a wave packet which is rapidly damped, and the flow reaches a steady state (Fig. 4a). By increasing Re_R , more and more time is needed to reach the steady flow and then, over the critical Reynolds number, exponential oscillatory growth of the disturbances appears (Fig. 4b). Finally, for higher Re_R , the flow reaches an asymptotic finite amplitude state. However, for some flows, a different pattern can be observed: At the beginning of the process, the wave packet is rapidly damped and the flow reaches a steady state (Fig. 6a) but for higher Re_R we do not observe oscillatory disturbances but only direct transition from a steady to chaotic state (Fig. 6c).

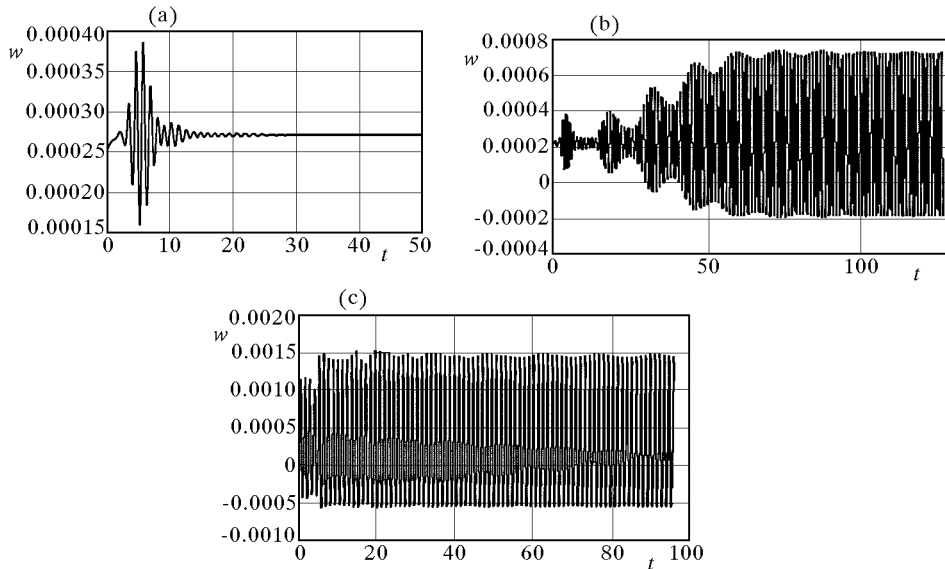


Fig. 4. Instability characteristics of the axial velocity component obtained for $L = 5$ and $R_m = 5$ in the monitoring point M , stator boundary layer, (a) $Re_R = 12000$, (b) $Re_R = 64000$, (c) $Re_R = 70000$

Basing on the 2D results by Daube *et al.* (2001), obtained for linear end-wall profiles, we expected direct transition from a steady flow to a chaotic flow for small R_m . On the other hand, the 3D results published by Serre *et al.* (2004) demonstrated that for a cylindrical cavity of the aspect ratio $L = 5$ ($R_m = 1.0$), a change in the end-wall condition from the linear profile to the exponential one, resulted in a shift from subcritical to supercritical transition. In the present section we performed calculations for $L = 5$ and different R_m (including R_m close to 1) and for two different end-wall boundary conditions, namely linear and exponential ones in order to check the influence of these conditions on the nature of the first bifurcation in the annular geometry.

5.3.1. Cases with exponential azimuthal end-wall velocity profiles

In this section, we consider the most unstable configuration: the internal end-wall attached to the rotor and the outer end-wall attached to the stator. The exponential azimuthal velocity end-wall profiles have been used. From the instability characteristics of the axial velocity component (Fig. 4) obtained for $L = 5$ and $R_m = 5$ (the monitoring point M , the stator boundary layer), we can see that, in this particular case, the transition to unsteadiness is oscillatory. We estimated the critical Reynolds number at $\text{Re}_R = 48500$ ($\sigma = 2\pi/T = 5.3$). Oscillatory solutions are observed in all monitoring points. Instantaneous iso-lines of disturbances of the azimuthal velocity are presented in Fig. 5. The disturbances in the boundary layer of the stationary disk are convected downstream towards the internal end-wall where they are lifted up to the rotating disk. Then, the disturbances are convected towards the outer end-wall. In the boundary layers of the stationary and rotating disks, we observed 6 and 2 vortices, respectively.

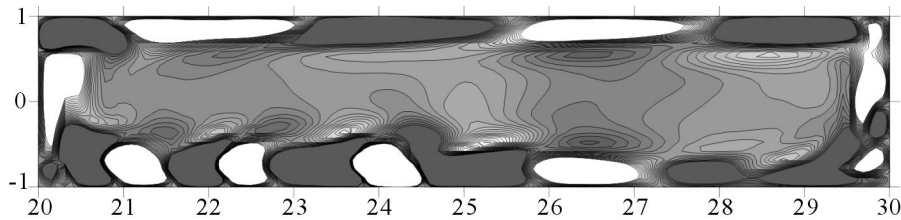


Fig. 5. Instantaneous iso-lines of disturbances of the azimuthal velocity component obtained for $R_m = 5$, $L = 5$, $\text{Re}_R = 64000$, in $(r^*/h, z)$ plane

A different pattern is observed for $R_m = 1.5$. At the beginning of the process (similarly to the case $R_m = 5.0$) disturbances introduced by a change in the rotation of the disk are very quickly damped and the flow reaches a steady state (Fig. 6). For higher Re_R , more and more time is needed to get a steady flow. However, over the critical Reynolds number (46500), we observe direct transition to unsteadiness. We did not observe any oscillatory solution. This is a hint that the transition to unsteadiness could be subcritical. In Fig. 7 we can see that only the boundary layer of the stationary disk is disturbed, whereas the rotating disk remains undisturbed. Disturbances at the stationary disk are amplified as they are convected towards the internal end-wall but at $r^*/h = 4$ they are rapidly damped. Very similar behaviour was observed in the cylindrical cavity (Serre *et al.*, 2004). Due to the existence of a stable area near the internal end-wall (Fig. 7) no disturbances are lifted up to the rotating disk, and the boundary layer of the rotating disk remains undisturbed.

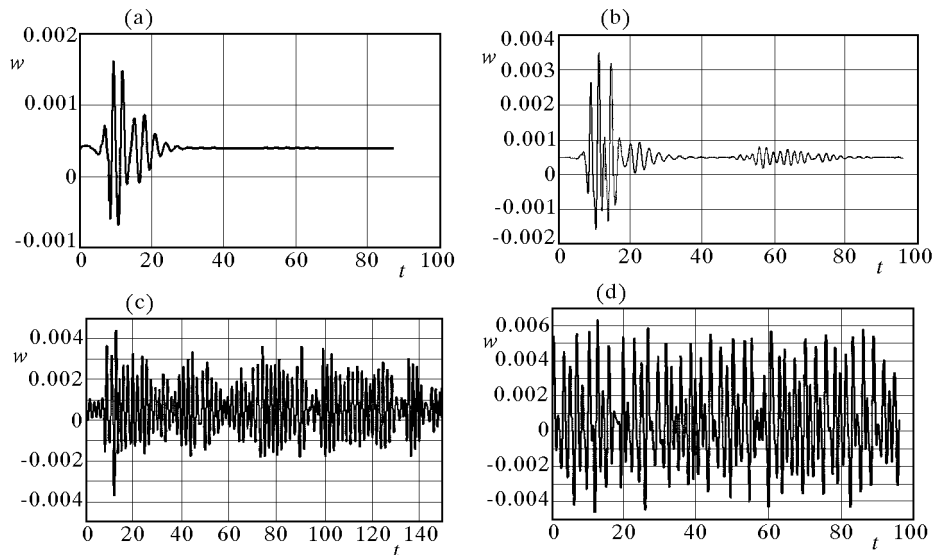


Fig. 6. Instability characteristics of the axial velocity component obtained for $L = 5$ and $R_m = 1.5$ in the monitoring point M , stator boundary layer, (a) $Re_R = 24000$, (b) $Re_R = 39000$, (c) $Re_R = 48000$, (d) $Re_R = 57000$

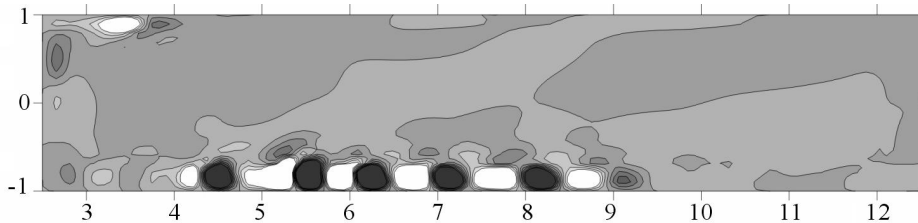


Fig. 7. Instantaneous iso-lines of disturbances of the azimuthal velocity component obtained for $R_m = 1.5$, $L = 5$, $Re_R = 57000$, in $(r^*/h, z)$ plane

5.3.2. Cases with linear azimuthal end-wall velocity profiles

In this section we analyse a solution obtained for $L = 5$ and $R_m = 1.5 - 6$ with linear end-wall azimuthal velocity profiles. These calculations have been undertaken to compare our results with computations performed by Daube *et al.* (2001), who analyzed nature of the first bifurcations for $L = 5$ and $R_0/R_1 = 0.99 - 0.1$ (these correspond to $R_m = 199 - 1.5$). Daube used in his calculations two methods: stream-function – vorticity formulation, and in the second version, velocity – pressure formulation with the Chebyshev spatial approximation (more details can be found in Daube *et al.*, 2001).

For linear azimuthal velocity end-wall profiles, an oscillatory solution appears in our calculations only for higher values of R_m . For $R_0/R_1 = 0.4$ ($R_m = 2.333$) in all monitoring points in the boundary layer of the stationary disk we observed that the disturbances are amplified, then they are damped and again amplified and damped. Finally, however, the flow reaches a stable state, which is visible in Fig. 8. These jumps of amplitudes are also observed in cases discussed in the previous Section but they were not so rapid. For $R_m = 2.333$, the critical Reynolds number of transition to unsteadiness was established to be about $Re_R = 55000$, which is close to Daube's result obtained for $Re_R = 6544$. The iso-lines of disturbances of the azimuthal velocity component obtained for $Re_R = 65000$ are presented in Fig. 9. We can see that only the boundary layer of the stationary disk is disturbed, where we observe 7 pairs of counter-rotating vortices. The angular frequency obtained for $Re_R = 65000$ equals $\sigma = 2\pi/T = 5.4$.

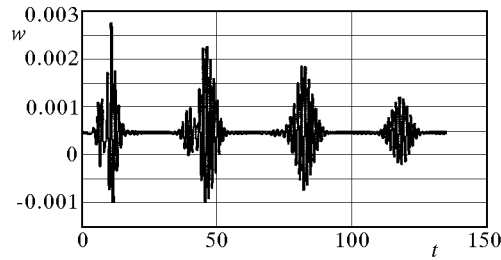


Fig. 8. An instability characteristic of the axial velocity component obtained in the monitoring point M in the boundary layer of the stationary disk; $R_m = 2.333$, $L = 5$, $Re_R = 48000$

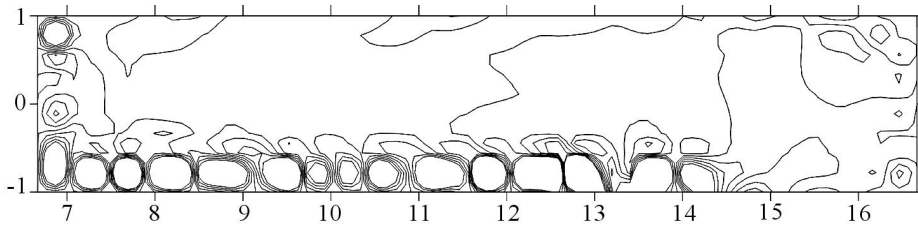


Fig. 9. Instantaneous iso-lines of disturbances the azimuthal velocity component obtained for $R_m = 2.333$, $L = 5$, $Re_R = 65000$, in $(r^*/h, z)$ plane

Instability characteristics obtained for $R_0/R_1 = 0.3$ ($R_m = 1.857$) are slightly chaotic. The critical Reynolds number of the transition to unsteadiness was established at $Re_R = 59000$. In the iso-lines of azimuthal disturbances (Fig. 10) we can see dislocations of vortices; two of ten disturbances are out.

The first dislocation we can see at $r^*/h = 5.4$ and the second one at $r^*/h = 7$. Similar dislocations were observed by Daube *et al.* (2001). The dislocations were reported for circular waves by Cousin-Rittemard (1996) in an annular rotating cavity of $L = 5$ and $R_m = 2$ at $39000 < \text{Re}_R < 56000$, and in an experimental investigation by Schouveiler *et al.* (1999).

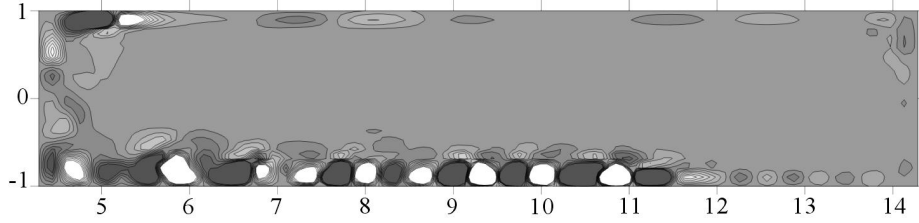


Fig. 10. Instantaneous iso-lines of disturbances of the azimuthal velocity component obtained for $R_m = 1.857$, $L = 5$, $\text{Re}_R = 65000$, in $(r^*/h, z)$ plane

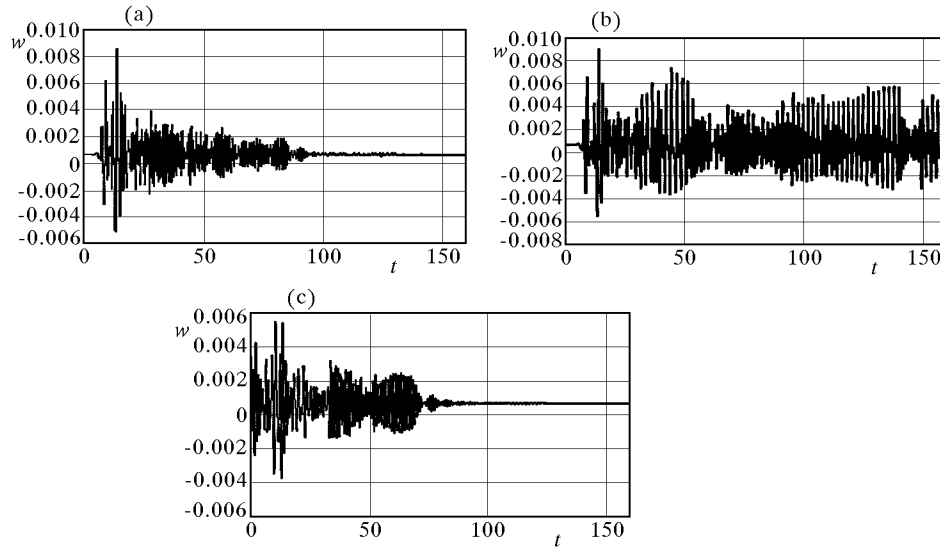


Fig. 11. Instability characteristics of the axial velocity component obtained for $R_m = 1.5$, $L = 5$, from the top to the bottom; (a) $\text{Re}_R = 65000$, (b) $\text{Re}_R = 68000$, (c) $\text{Re}_R = 64000$, the initial condition from 68000

For $R_0/R_1 = 0.2$ ($R_m = 1.5$), the critical Reynolds number of transition to unsteadiness lies somewhere between $\text{Re}_R = 65000$ and 68000 (see Fig. 11). Figure 11 shows that for $\text{Re}_R = 65000$, the flow reaches a steady state at $t \approx 100$, and for $\text{Re}_R = 68000$ the flow is unsteady and apparently chaotic. In

this case, we did not observe an oscillatory solution but only direct transition from the steady to chaotic flow. It indicates that the first bifurcation can be subcritical. In the next step, we checked if some hysteresis could be present. For this purpose, the instantaneous state which was obtained for $\text{Re}_R = 68000$, was used as the initial condition for the case $\text{Re}_R = 64000$. As can be seen in Fig. 11c, the flow reverted to a steady state at $t \approx 120$, and therefore, no hysteresis could be detected in the considered range of the Reynolds number. This result indicates that transition to unsteadiness is subcritical, which is in agreement with the experimental results by Schouveiler et al (1999) and Gauthier *et al.* (1999).

6. Conclusions

A incompressible fluid flow in an annular rotor/stator configuration with different aspect ratios L and curvature parameters R_m has been numerically investigated. The efficient spectral collocation method enabled accurate investigation of the first stage of transition to turbulent flow. We focused attention on the influence of the end-wall conditions on instability structures of the flow and on the nature of the first bifurcation to unsteadiness. Calculations performed for $L = 4$ and $R_m = 5$ showed dramatic influence of different approximations of end-wall azimuthal velocity profiles on the instability structures in both boundary layers. The most unstable turns out to be the flow with exponential velocity end-wall profiles and with the internal end-wall attached to the rotor and with the outer one attached to the stator. The spectral parameters of vortices propagating in the boundary layers have been given.

Calculations performed for $L = 5$ and different $R_m = 1.5 - 6.0$ with linear azimuthal end-wall profiles showed good agreement with the results by Daube *et al.* (2001) performed for the same geometry. We have found the classical scenario of transition to unsteadiness (with an oscillatory solution) for higher R_m . For smaller R_m , however, the first bifurcation seems to be subcritical. For linear profiles and for smaller R_m , we observed dislocations on the iso-lines of vortices in the boundary layer of the stationary disk.

Similar series of 2D calculations, carried out for exponential end-wall velocity profiles with the outer end-wall attached to the stator and with the inner end-wall attached to the rotor, again showed oscillatory transition to unsteadiness at higher R_m and direct transition from a steady flow to chaotic one at very small R_m . In the annular cavity, the change of the azimuthal end-wall

profiles from linear to exponential did not result in a change of the nature of the first bifurcation, which was observed by Serre *et al.* (2004) where a 3D flow in a cylindrical cavity of the aspect ratio $L = 5$ was investigated. Additionally, our primary calculations of the 3D flow in an annular cavity have shown large influence of three-dimensionality on the instability structures but rather small on the nature of the first bifurcation.

Further 3D calculations are necessary to clarify the problem of the nature of the first bifurcation. The study on this subject and also on the absolute/convective character of the instability in both the rotor/stator (considered in this paper) and rotor/rotor cavity with throughflow is in progress.

References

1. ADAMS M.L., SZERI A., 1982, Incompressible flow between finite discs, *J. Appl. Mechanics*, **49**, 1-9
2. CANUTO C., HUSSAINI M.Y., QARTERONI A., ZANG T.A., 1988, *Spectral Methods in Fluids Dynamics*, Springer
3. CALDWELL D.R., VAN ATTA C., 1970, Characteristics of Ekman boundary layer instabilities, *J. Fluid Mech.*, **44**, 79-95
4. COUSIN-RITTEMARD N., 1996, Contribution a l'étude des instabilités des écoulements axisymétriques en cavité inter-disque de type rotor-stator. Doctorate Thesis, Université de Paris VI
5. COUSIN-RITTEMARD N., DAUBE O., LE QUÉRÉ P., 1998, Sur la nature de la première bifurcation des écoulements interdisques, *C. R. Acad. Sci.*, serie IIb, **326**, 359-366
6. DAUBE O., LE QUÉRÉ P., COUSIN-RITTEMARD M., JACQUES R., 2001, Influence of curvature on transition to unsteadiness and chaos of rotor-stator disk flows, submitted to *J. Fluid Mech.*
7. DIJKSTRA D., HEIJST G., 1983, The flow between finite rotating discs enclosed by a cylinder, *J. Fluid Mech.*, **128**, 123-154
8. FALLER A.J., 1963, An experimental study of the instability of the laminar Ekman boundary layer, *J. Fluid Mech.*, **15**, 560-576
9. GAUTHIER G., GONDRET P., RABAUD M., 1999, Axisymmetric propagating vortices in the flow between a stationary and a rotating disk enclosed by a cylinder, *J. Fluid Mech.*, **386**, 105-127

10. HALDENWANG P., LABROSSE G., ABBOUDI S., DEVILLE M., 1984, Chebyshev 3D spectral 2D pseudospectral solver for the Helmholtz equation, *J. Comput. Phys.*, **55**, 115-128
11. ITOH M., 1991, On the instability of the flow between coaxial rotating disks, In: *Boundary Layer Stability and Transition to Turbulence*, ASME FED-Vol. 114, 83-89
12. KOBAYASHI R., KOHAMA Y., TAKAMADATE CH., 1980, Spiral vortices in boundary layer transition region on a rotating disk, *Acta Mechanica*, **35**, 71-82
13. LINGWOOD R., 1995, Absolute instability of the boundary layer on a rotating disk, *J. Fluid. Mech.*, **299**, 17-33
14. LINGWOOD R., 1996, Experimental study of absolute instability of the rotating-disk boundary layer flow, *J. Fluid. Mech.*, **314**, 373-405
15. LINGWOOD R., 1997, Absolute instability of the Ekman layer and related rotating flows, *J. Fluid. Mech.*, **331**, 405-428
16. OLIVEIRA L.A., PECHEUX J., RESTIVO A.O., 1991, On the flow between a rotating and a coaxial fixed disc: numerical validation of the radial similarity hypothesis, *Theoret. Comp. Fluid Dyn.*, **2**, 211-221
17. SAVAS O., 1987, Stability of Bödewadt flow, *J. Fluid Mech.*, **183**, 77-9
18. SCHOUVEILER L., LE GAL P., CHAUVE M. P., TAKEDA Y., 1999, Spiral and circular waves in the flow between a rotating and a stationary disc, *Experiments in Fluids*, **26**, 179-187
19. SERRE E., CRESPO DEL ARCO, BONTOUX P., 2001, Annular and spiral patterns in flow between rotating and stationary disks, *J. Fluid. Mech.*, **434**, 65-100
20. SERRE E., PULICANI J., 2001, A three-dimensional pseudospectral method for rotating flows in a cylinder, *Computers and Fluids*, **30**, 491-519
21. SERRE E., TULISZKA-SZNITKO, BONTOUX P., 2004, Coupled numerical and theoretical study of the flow transition between a rotating and stationary disk, *Phys. of Fluids*, **16**, 3
22. TULISZKA-SZNITKO E., SOONG C-Y., 2000, Instability of non-isothermal flow between coaxial rotating disks, *Proceedings of European Congress on Computational Methods in Applied Sciences and Engineering*, Barcelona
23. TULISZKA-SZNITKO, SERRE E., BONTOUX P., 2002, On the nature of the boundary layers instabilities in a flow between a rotating and a stationary disc, *C.R. Mecanique*, **30**, 90-99

Badanie metodą symulacji numerycznej charakteru pierwszej bifurkacji przepływu pomiędzy wirnikiem i stojanem

Streszczenie

W pracy badana jest stabilność przepływu w wirującej, pierścieniowej przestrzeni pomiędzy wirnikiem i stojanem metodą bezpośrednią. Zagadnienie przepływu w przestrzeniach pomiędzy tarczami wirującymi w różnych konfiguracjach jest istotne nie tylko ze względów poznawczych, ale również aplikacyjnych. Tego typu przepływy występują pomiędzy tarczami silników turbogazowych i sprężarek osiowych. Zagadnienie może zainteresować w szczególności inżynierów zajmujących się chłodzeniem tarcz silników turbogazowych. Z punktu widzenia teoretycznego jest bardzo interesujące poznanie szeregu kolejnych bifurkacji prowadzących w wirujących przestrzeniach od przepływu laminarnego do turbulentnego. Analizowany jest wpływ bezwymiarowych parametrów geometrycznych przestrzeni, tj. współczynnika rozciągłości obszaru L , parametru krzywizny R_m , jak i wpływ warunków brzegowych stawianych na pierścieniach ograniczających przestrzeń na charakter pierwszej bifurkacji. Badane są struktury niestabilnościowe występujące w warstwach przyściennych wirnika i stojana. Do badań zastosowano metodę spektralnej kolokacji bazującą na szeregach Czebyszewa. Zastosowany schemat po czasie jest kombinacją schematu wstecznego o dokładności drugiego rzędu i schematu Adamsa-Bashfortha.

Manuscript received June 15, 2004; accepted for print October 18, 2004